Velocity dependence of energy pooling collisions in strontium

J. A. Neuman, J. Cooper, and A. Gallagher
JILA, National Institute of Standards and Technology and the University of Colorado, Boulder, Colorado 80309-0440
(Received 21 February 1997)

The threshold behavior of the cross section of an endothermic energy pooling reaction is investigated. In a vapor cell experiment, pulsed excitation followed by delayed fluorescence detection narrows the transverse velocity distribution of colliding pairs of laser-excited strontium atoms in the $5s5p\,^3P_1$ level, and laser detuning establishes the collision velocity in the direction of counterpropagating laser beams. A probe laser detects the excited-state collision product of the endothermic $5s5p\,^3P_1+5s5p\,^3P_1\rightarrow 5s6s\,^1S_0+5s^2\,^1S_0$ reaction. The cross section rises steeply at threshold and is nearly flat for 1.2–2 times the threshold energy. This behavior can be partly explained by the shape of the molecular potential curve of the collisionally produced state. From the measured 1.1×10^{-12} cm^3 s^{-1} thermally averaged rate coefficient, the above-threshold cross section is found to be approximately 6×10^{-17} cm^2. The thermally averaged rate coefficient for the highly exothermic energy pooling reaction $5s5p\,^3P_1+5s5p\,^3P_1\rightarrow 5s5p\,^1P_1+5s^2\,^1S_0$ is also reported and measured to be 1.1×10^{-10} cm^3 s^{-1}. The cross section for this exothermic reaction is found to be nearly independent of collision velocity. [S1050-2947(97)04707-0]

PACS number(s): 34.30.+h, 34.50.−s, 82.20.Pm

I. INTRODUCTION

Atomic collisions that induce electronic excitation transfer have been studied for over three decades, and energy pooling (EP) collisions between pairs of excited atoms have received considerable attention for about a decade. EP refers to the transfer of electronic energy when two excited atoms collide to produce one highly excited atom and one ground-state atom. These collisions are of current interest [1] because they may represent important loss mechanisms and trap diagnostics for optically trapped atoms [2]. Experimental investigations of EP reactions offer a powerful method for examining inelastic collision processes, since both collision partners are optically excited. This offers the possibility to control collision parameters such as orbital alignment and collision velocity. In atoms with two electrons in the outer shell, such as strontium used here, many energy levels are accessible to EP and angular momentum changes in an EP reaction can be studied. In the past, we [3] and others [4] have reported the dependence of EP upon spin and orbital angular momentum changes and energy defect, yet clear trends that might lead to an explanation of these results have been elusive. Since EP rate coefficients are often measured to be large but are mostly unexplained, more sensitive experiments are necessary to elucidate the physical processes important in these collisions. Energy pooling experiments that control collision velocity are particularly attractive for their ability to yield new insights into excitation transfer [5].

This study investigates an EP process in strontium and also advances experimental capabilities. The measurement of the velocity dependence of a cross section tests the threshold behavior of an endothermic reaction and reveals the experimental velocity resolution. A technique, which is applicable to experimentation in many different elements, accurately defines the collision velocity in a vapor cell. Isotopically enriched strontium is used, so that the severe complications from multiple velocity groups due to hyperfine and isotopic splittings are eliminated.

When translational kinetic energy is converted to electronic energy in the endothermic reaction

$$\mathrm{Sr}(5s5p\,^3P_1)+\mathrm{Sr}(5s5p\,^3P_1)\rightarrow \mathrm{Sr}(5s6s\,^1S_0)+\mathrm{Sr}(5s^2\,^1S_0)-1583\ \mathrm{cm}^{-1}, \quad (1)$$

the production of the $5s6s\,^1S_0$ level (called the $6\,^1S$ level below) must be zero for collision energies below the 1583 cm^{-1} ($\sim 3kT$) endothermicity (Fig. 1). This feature of the collision cross section assists in determining the velocity

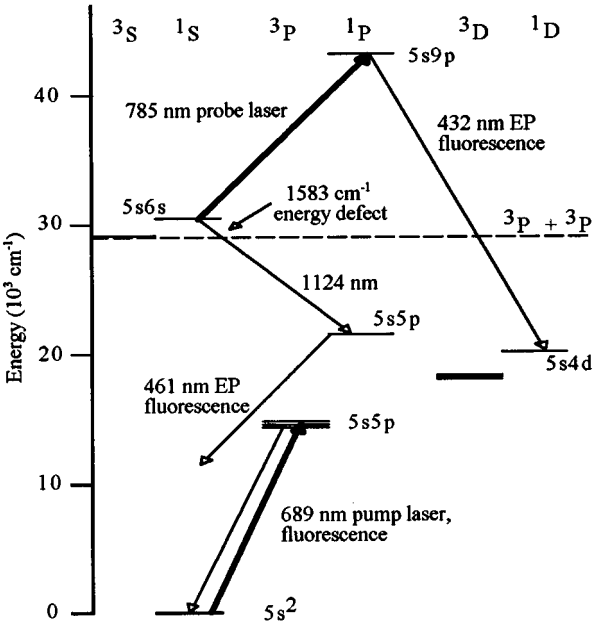

FIG. 1. Strontium energy-level diagram, with pump, probe, and detection transitions shown.

resolution achieved by the experiment and serves as a valuable experimental check. The highly exothermic EP reaction,

$$\mathrm{Sr}(5s5p\,^3P_1)+\mathrm{Sr}(5s5p\,^3P_1) \rightarrow \mathrm{Sr}(5s5p\,^1P_1)+\mathrm{Sr}(5s^2\,^1S_0)+7310\ \ \mathrm{cm}^{-1}, \tag{2}$$

which was previously assumed not to occur as a consequence of the large energy defect [6], has also been observed. By using a probe laser to separately defect the $6\,^1S$ collision products, we clear up confusion regarding the production of the $5s5p\,^1P_1$ level (called $5\,^1P$ below) from the collision of pairs of atoms in the $5s5p\,^3P_1$ level (called $5\,^3P$ below). Thermal rate coefficients and the velocity dependence to the collision cross sections for reactions (1) and (2) are determined.

A complete collisional model would include curve-hopping probabilities for the many molecular states that could be involved in the collision. Such a calculation is not yet possible, since all the potential energy curves for excited pairs of strontium atoms have not been determined [7]. However, some reasonable predictions regarding curve-hopping probabilities and the shape of the molecular potential curve of the exit channel for Eq. (1) can be made based upon the measured energy dependence of the cross section. A mathematical model that includes the effects of the transverse velocity distribution of excited atoms is used to determine the energy dependence of the collision cross section from the data. Different theories for the energy dependence of a cross section for an endothermic reaction are then compared to the results.

II. VELOCITY SELECTION IN A CELL

The Doppler effect can be exploited to produce velocity-selected laser-excited atoms in the direction of the laser (z direction). This technique has been used for decades in atomic physics, and it is sometimes called velocity-selected Doppler shift (VSDS) [8]. A narrow linewidth laser selectively excites a narrow velocity group in the z direction from the thermal (Maxwellian) distribution of atomic velocities in the cell. According to the Doppler effect, $\delta = k v_z$, where $k = 2\pi/\lambda$, δ is the laser detuning from the atomic resonance, and v_z is the velocity component of the excited atom. Counterpropagating beams sent through the cell excite velocity groups $v_z = \pm \delta/k$, so that the collision velocity in the z direction is $\Delta v_z = 2\delta/k$.

But without further manipulation of the atoms, the collision velocity in the transverse direction is still determined by a thermal distribution of atoms, contributing $\sim kT$ of energy width to the collision. This contribution from transverse velocities ($v_\perp$) to the EP collision energy is reduced by pulsing the laser and waiting for the atoms with large $v_\perp$ to leave the detection volume. Following the excitation of a small volume of atoms by a short pulse of focused laser light, the density of excited atoms decreases more rapidly for atoms with large $v_\perp$ than for atoms with small $v_\perp$. After a sufficient time (Δt) following the end of the laser pulse, only atoms with small $v_\perp$ contribute to the EP collision. The 21-μs lifetime [9] of the $5\,^3P$ level allows measurement of EP signals at large Δt, when most $5\,^3P$ atoms with large $v_\perp$ have left the detection volume. But as the laser-excited atoms spread, the density of colliding atoms and the EP collision rate decrease, and this reduces the signal and limits the useable Δt.

If collisions occur between atoms with negligibly small $v_\perp$, the total collision velocity will be determined mostly by Δv_z, which is established by δ. In this experiment, the laser frequency is intentionally chirped in order to effectively broaden the laser slightly (described below). Velocity resolution is defined here to mean the extent to which the total collision velocity is determined by δ, the laser detuning without chirping. In the laser direction, the collision energy E_z is determined by δ according to $E_z = (\mu/2)(\Delta v_z)^2 = (\mu/2)(2\lambda\delta/k)^2$, where μ is the reduced mass of the strontium atoms. If atoms collide with negligible $v_\perp$, then the threshold detuning for a collision energy that overcomes the 1583-cm^{-1} energy barrier is 671 MHz. The 8-kHz natural linewidth of the $5\,^3P$ level contributes a negligible spread to the excited v_z velocity group, compared to the 970-MHz Doppler width and the 671-MHz threshold. Hence, good velocity resolution is evidenced by an EP rate that is zero for $\delta < 671$ MHz.

We use a mathematical model to account for the $v_\perp$ contribution to the measured EP signal, so that the energy dependence of the cross section can be established from the data. The measured EP collision rate $R(\delta,\Delta t)$, including the time dependence of the laser excitation and integrals over atomic velocities and spatial coordinates, has the form

$$\begin{aligned} R(\delta,\Delta t) \propto & \int_0^\infty v_1 dv_1 e^{-mv_1^2/2kT} \int_0^\infty v_2 dv_2 e^{-mv_2^2/2kT} \\ & \times \int_{-\infty}^\infty dv_{z1} e^{-mv_{z1}^2/2kT} \int_{-\infty}^\infty dv_{z2} e^{-mv_{z2}^2/2kT} \\ & \times \int_0^a r\ dr\ \sigma(v_c) v_c \frac{n_1^*}{n_1}(\mathbf{v}_1,\Delta t,r,v_{z1},\delta) \\ & \times \frac{n_2^*}{n_2}(\mathbf{v}_2,\Delta t,r,v_{z2},\delta), \end{aligned} \tag{3}$$

where v_c is the total collision velocity defined by $v_c = (\Delta v_z^2 + |\mathbf{v}_1 - \mathbf{v}_2|^2)^{1/2}$. The velocity of each atom perpendicular to the laser is labeled by $\mathbf{v}_1$ and $\mathbf{v}_2$, and the velocity in the z direction is denoted by v_{z1} and v_{z2}. The velocity-dependent collision cross section for EP is $\sigma(v_c)$, and n'/n is the probability that an atom is laser-excited from the ground state. The volume integral is over the detection volume of radius a, rather than the entire cell, since this experiment measures EP with a probe laser of radius a. The laser beam actually has a nearly Gaussian shape, though it is treated as a step here to simplify the calculations. An exact solution of Eq. (3) requires consideration of correlations between the $\mathbf{v}_\perp$ of the two particles: Since both particles must be at the same place at the same time for a collision to occur, the position and velocity of one particle establishes constraints upon the other particle. Here we ignore that correlation and assume the EP rate is the product of the densities of the laser-excited atoms that are in the detection volume at

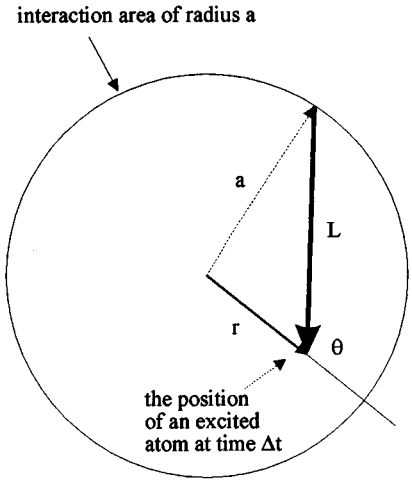

FIG. 2. An excited atom at time Δt, radial position r, and angle θ within the detection volume of radius a. θ is the angle that vector **r** makes with respect to the vector **L**. The direction of the laser is perpendicular to the plane of the page. Given the position of the excited atom, the distance L is determined from the law of cosines, and then τ_{laser} is found with Eq. (4).

Δt, and for simplicity we take $|\mathbf{v}_2-\mathbf{v}_1|^2=v_2^2+v_1^2$. The excitation probability n^*/n is in general a complicated function of time, position, and velocity. However, there are some simplifications that make the problem tractable.

A correct representation of n^*/n must account for the probability that an atom is excited as a function of the time it interacts with the laser field (τ_{int}). Since the $5\,^3P$ level's 21-μs radiative lifetime is much longer than the $\sim$1-μs excitation pulse width, it is appropriate to ignore radiative decay and solve the Schrödinger equation to find the τ_{int} dependence of the probability amplitude for exciting an atom to the $5\,^3P$ level. The treatment of the excitation of a two-level atom by coherent radiation appears in many quantum optics texts [10], but must be modified here to include a frequency-modulated laser and the velocity-dependent Doppler shift for each atom. Due to the very narrow natural linewidth of this $5\,^3P$ excitation (8 kHz), a small fraction of atoms are excited by a single-frequency laser. Therefore, the pump laser is frequency modulated across a 20-MHz range by applying a 1-MHz sinusoidal modulation to the diode laser current. This excites a 14-m/s-wide v_z velocity group that is still narrow compared to the 670-m/s Doppler width and the 925-m/s threshold velocity. A numerical solution is found for the probability of exciting an atom as a function of laser detuning and τ_{int}.

A geometrical picture is constructed to use this τ_{int} dependence of excitation to obtain n^*/n used in Eq. (3) as a function of transverse velocity $v_\perp$ and time Δt after the laser pulse is off. This analysis considers the constraints placed upon τ_{int} and $v_\perp$ if an excited atom resides in the detection volume at Δt, and these constraints establish n^*/n. τ_{int} can be found with Fig. 2, which shows an excited atom that has traveled a distance L through the laser beam and is at position $r<a$ at time Δt. Using Fig. 2, the law of cosines, and the quadratic formula, it is possible to find the time (τ_{laser}) that an excited atom is in the detection volume defined by the laser beam:

$$\tau_{\text{laser}}(r,\theta,v_\perp,\Delta t)=\frac{r}{v_\perp}\left(-\cos(\theta)+\sqrt{(a/r)^2-\sin^2(\theta)}\right)-\Delta t. \tag{4}$$

Since $\tau_{\text{laser}}<0$ for large $v_\perp$ or Δt, limits must be placed on τ_{laser} in order to guarantee that it meaningfully represents the true interaction time τ_{int}. Physically, $\tau_{\text{laser}}<0$ represents an excited atom that has left the interaction region and is no longer observable, and the excited-state density within the detection volume is set to zero in this case. While Fig. 2 and the accompanying equations illustrate an atom that starts outside the interaction region at the beginning of the laser pulse, atoms that start inside the detection volume at the beginning of the laser pulse can also be treated with these equations. This is handled by setting τ_{int} equal to the pulse time τ_p when the solution to Eq. (4) is greater than τ_p. Thus, the equation for τ_{int} is

$$\tau_{\text{int}}(r,\theta,v_\perp,\Delta t)=\begin{cases}0, & \tau_{\text{laser}}<0\\ \tau_{\text{laser}}, & 0<\tau_{\text{laser}}<\tau_p\\ \tau_p, & \tau_{\text{laser}}>+\tau_p.\end{cases} \tag{5}$$

An average over θ gives $\tau_{\text{int}}(r,\Delta t,v_\perp)$, and this is used with the calculated τ_{int} dependence of the probability of excitation to find n^*/n. With this formulation for the density of excited-state atoms, the EP rate can be found from Eq. (3) by integrating over the detection volume and transverse velocities. The apparent rate coefficient k_a is the calculated EP rate divided by the number of collision pairs at a given laser detuning.

The essence of pulsed excitation and delayed fluorescence detection can be illuminated by explicitly examining the calculated narrowing of the transverse velocity distribution. Time-dependent transverse velocity distributions of laser-excited atoms are determined from the two-dimensional $n^*(v_\perp,\Delta t)/n$ distribution of atoms remaining in the interaction region. The $n^*(v_\perp,\Delta t)/n$ are shown for $v_0\Delta t/a=2.3$ (thick line) and for $v_0\Delta t/a=0.39$ (thin line) in Fig. 3, where $v_0=(2kT/m)^{1/2}$. The collisional energy spread is proportional to the spread in $v_\perp^2$, which has narrowed from kT to $\sim 0.14kT$ for the $v_0\Delta t/a=2.3$ case shown.

The excess kinetic energy (amount above threshold) in this endothermic reaction of two $5\,^3P$ atoms determines the velocity distribution of the $6\,^1S$ collision products. If a narrow-linewidth laser were used to probe the $6\,^1S$ level, atoms with large velocities in the z direction would be Doppler shifted out of resonance with the probe laser and would go undetected. This would bias the data to under-represent large collision velocities, for which the collisionally produced $6\,^1S$ atoms have greater kinetic energy and velocity. For this reason, the probe laser frequency is phase modulated so that the laser frequency is effectively broadened and there is a nearly constant probe excitation over the whole range of final velocities of interest.

The loss rate of the collisionally produced $6\,^1S$ atoms from the detection volume is also velocity dependent. If atoms populated by EP travel out of the laser interaction region before being detected, those created at large pump laser detunings with greater excess kinetic energy have a higher loss rate and are under-represented by the probe laser detection. However, since the $6\,^1S$ atoms radiatively decay much

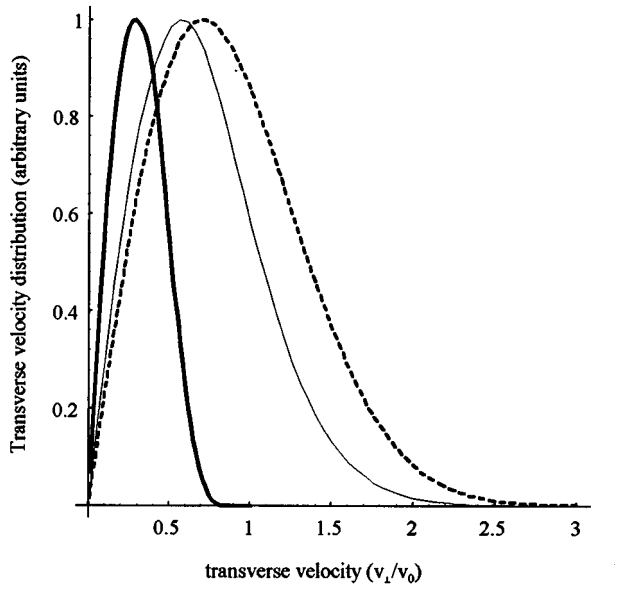

FIG. 3. The transverse velocity distribution for a thermal vapor (dashed line) and for a pulsed excitation and delayed fluorescence detection experiment with little narrowing of the transverse velocity (thin line) and with considerable narrowing (thick line). All distributions have been normalized to 1 at their peak for ease of comparison.

faster ($\tau_{\rm nat}=54$ ns) than they travel out of the interaction region (~ 300 ns for $v_\perp = v_0$), it is possible to ignore the effect of the transverse velocity of the EP collision products upon the measured EP signal. Similarly, atoms produced by EP outside the detection region that travel back into the detection region do not significantly contribute to the observed EP rate. Just as the radiative decay rate of $6\,^1S$ atoms exceeds the rate at which they leave the detection volume, it also exceeds the rate of return to the interaction region.

III. EXPERIMENTAL DETAILS

This experiment utilizes many of the well-documented and successful designs for constructing narrow-linewidth tunable diode lasers [11] for spectroscopy experiments. Strontium atoms are excited from the ground state to the $5\,^3P$ excited state by a grating-feedback controlled $Al_xGa_{1-x}InP$ diode laser (pump laser) tuned to the 689-nm intercombination line. A second diode laser (probe laser) is tuned to the 785-nm $6\,^1S \rightarrow 9\,^1P$ transition from the collisionally produced excited state, as shown in Fig. 1.

The 689-nm light is generated by an antireflection (AR) coated [12] visible diode laser placed in a temperature-controlled, grating-terminated external cavity. The external cavity narrows the linewidth and increases the tunability of the laser, and the AR coating on the diodes prevents the diode cavity from acting as an etalon within the external cavity defined by the diffraction grating and the rear facet of the diode laser. After the front facets of the lasers were AR coated with approximately 700 Å of Al_2O_3 and 600 Å of Hf_2O_2, the diode lasers could be tuned continuously more than 15 GHz by applying a voltage to a piezoelectric disk that moves the diffraction grating. The pump laser injection current is modulated at a rate of 10 MHz and at an amplitude that produces a 20-MHz full width at half maximum (FWHM) spectral width. When the pump laser is tuned across the intercombination line, a stable reference cavity provides frequency markers (with 5-MHz width) separated by 250-MHz intervals, and the saturated absorption dip provides an absolute frequency marker at zero detuning.

The pump laser is pulsed on for 1 μs with an acousto-optic modulator (AOM) at a repetition rate of 250 kHz. A pulse generator with a rise time less than 5 ns triggers the AOM and simultaneously triggers a transient digitizer used for data collection. After the AOM, a beam splitter divides the pump laser (Fig. 4), and counterpropagating beams are focused to a 150 μm$\times$300 μm spot within the 1.3-cm-long, 0.4-cm-diam sapphire cell (Fig. 5). The beams diverge by $\sim 1°$ to prevent unwanted feedback into the diode laser.

Since the collisionally produced atoms that are probed can have a broad frequency distribution ($\sim$1-GHz FWHM for the largest collision energy probed here), a broadband, high-power probe laser excites the most atoms and yields the best signal. The 785-nm probe laser is a $Ga_xAl_{1-x}As$ diode laser run without an external cavity, and tuning is achieved by changing the diode temperature and injection current. The output from a 50-MHz oscillator is added to the laser current, with a modulation amplitude sufficient to yield multiple sidebands across $\sim$1-GHz full width, as confirmed by a spectrum analyzer. Current pulses from a photomultiplier tube (PMT) with a rise time less than 10 ns were also added to the laser current, and the rate (light incident upon the PMT) and amplitude (gain on the PMT) of the pulses were adjusted to produce a smooth 1.2-GHz FWHM frequency spectrum. While Newsom *et al.* [13] measure the wavelength in air of the $6S \rightarrow 9P$ transition to be 785.00 nm (and this has been reproduced in many wavelength tables), we have determined the wavelength in air to be 784.963 (± 0.006) nm, which is consistent with the energy levels tabulated by Moore [14]. Our wavelength measurements were made by comparing fringes produced by a traveling-wave interferometer from a helium-neon laser to that of the diode laser.

Energy pooling fluorescence at 432 or 461 nm and intercombination fluorescence at 689 nm are monitored simultaneously. The blue EP fluorescence is measured and the 689-nm fluorescence is rejected with interference filters with $\sim$10-nm bandwidths placed in front of a CsSb bialkali PMT (quantum efficiency$\approx$25%). The 689-nm intercombination-line fluorescence is monitored through a fiber optic bundle connected to a 1/4-m monochromator with a PMT at the exit slit. The PMT's are connected to a fast amplifier-discriminator that gives 8-ns pulses, and this output is fed to a transient digitizer. Photon counting is necessary to record the weak EP signals. The EP-detecting PMT has a background of 200 counts/s, and typical EP signals at $\Delta t \sim 0.4$ μs are on the order of 300 counts/s. Scattered laser light from the pump laser produces square pulses with rise and fall times of $\sim$40 ns.

This experiment uses a high-temperature ultrahigh-vacuum optical cell that operates without a buffer gas and withstands high densities of extremely corrosive alkaline-earth metal vapors (Fig. 5). Since these strontium vapors rapidly attack hot Pyrex or quartz cell windows as well as copper gaskets and brazes, the cell is constructed from sap-

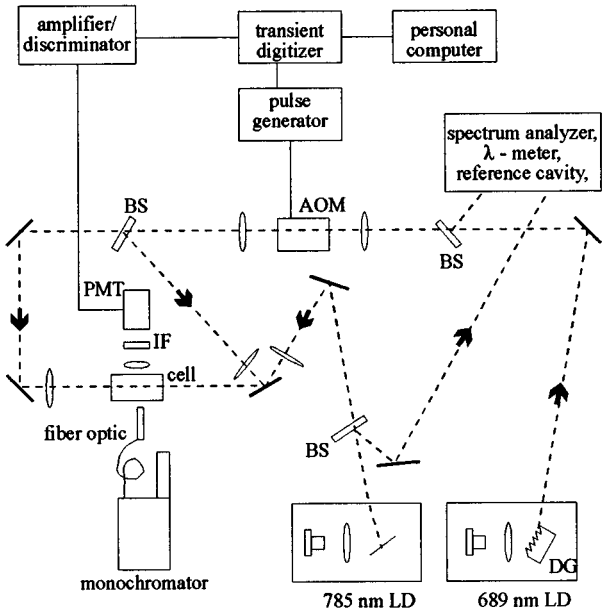

FIG. 4. Experimental apparatus, with laser diode (LD), diffraction grating (DG), acousto-optic modulator (AOM), and beam splitters (BS).

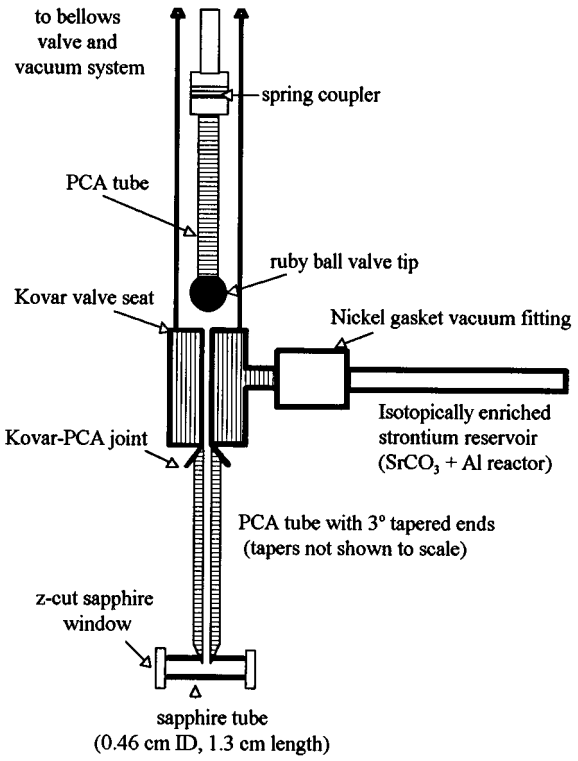

FIG. 5. Strontium vapor cell.

phire and polycrystalline alumina, which do not react with strontium at the temperatures and densities employed here. By melting glass powder between adjoining parts, we construct a compact and robust cell with hot windows that allow for a constant temperature and vapor density along the length of the cell. Also, this design permits light collection over a large solid angle, improving detection of the low EP light intensities emitted from the cell. The valve is the coldest spot in the cell, and its temperature determines the equilibrium vapor pressure. Low-power absorption of the pump laser tuned to the intercombination line is on the order of 50% and indicates a density of 3×10^{13} cm^{-3} at a temperature of 850 K, which is within 20% agreement of the Nesmayanov tables [15]. Further details regarding the assembly of sapphire cells, including the handling of the specific materials used, have been previously reported [16].

In any VSDS experiment, different isotopes or hyperfine components may be excited with different velocities, severely complicating the collisional velocity distribution. For strontium, there are four naturally occurring isotopes, each with an isotope shift. For this reason, isotopically enriched ^{88}Sr, which is readily available in carbonate form with $>$99.5% purity, is used. $SrCO_3$ can be reduced to Sr metal under vacuum by alumino-thermic reduction [17]. The carbonate is mixed with high purity aluminum powder and placed in a steel tube connected to high vacuum. Heating the carbonate to 800 °C releases CO_2 in the reaction $SrCO_3\rightarrow CO_2+SrO$, and at 950 °C, the reaction $3SrO+2Al\rightarrow Al_2O_3+3Sr$ occurs. Saturated absorption spectroscopy shows that the isotopically enriched Sr vapor we produce is greater than 99.5% ^{88}Sr.

IV. RESULTS

A. Velocity dependence of EP to the $5\,^1P$ level

Energy pooling fluorescence is observed from the $5\,^1P$ level of strontium when the $5\,^3P$ level is excited. Since the $6\,^1S$ level radiatively decays entirely to the $5\,^1P$ level, EP fluorescence from the $5\,^1P$ level represents the sum of EP transfer to the $6\,^1S$ level and the $5\,^1P$ level. This rate coefficient was measured [6], and the EP fluorescence was assumed to originate from a cascade from the $6\,^1S$ level due to the large energy defect to the $5\,^1P$ level. This assumption was made since previous EP experiments in strontium and other elements [3,4] had not detected EP with large energy defects as in Eq. (2), and there was no prior evidence for unusually repulsive or attractive potential curves that might lead to such a collision.

The apparent EP rate coefficient measured here is proportional to the ratio of the collision products to collision partners, which is represented by the EP fluorescence signal divided by the square of the increase in 689-nm fluorescence from the $5\,^3P$ level during the laser pulse. When the EP signal is 461-nm fluorescence from the $5\,^1P$ level, the rate coefficient is nearly independent of collision velocity (less than 10% variation for collision velocities from 30 to 1400 m/s), whereas the rate coefficient is expected to peak at large collision velocities if this EP fluorescence is from the exothermic excitation of the $6\,^1S$ level or any other higher-lying energy level. (The next-nearest energy level to the $6\,^1S$ level that could possibly cascade to the $5\,^1P$ level is the $4d5p\ ^3F$ level, which has a $+4600$-cm^{-1} energy defect.) Thus, the $5\,^1P$ fluorescence apparently is dominated by direct EP from a pair of $5\,^3P$ atoms, and a different detection scheme must be chosen to measure EP to the $6\,^1S$ level. Because the 1.1-μm direct fluorescence from the $6\,^1S$ level is difficult to detect for these weak signals, a 785-nm probe laser is tuned to the $6\,^1S\rightarrow9\,^1P$ transition, and the 432-nm fluorescence from the $9\,^1P$ level is used to separately indi-

cate population in the $6\,^1S$ level (Fig. 1). The intensity of the 461-nm EP fluorescence from the $5\,^1P$ level is unaffected ($<0.1\%$ change) by the probe laser, even when the probe laser strongly saturates the $6\,^1S \rightarrow 9\,^1P$ transition. We show below that this occurs because the 461-nm resonance fluorescence almost entirely ($>99\%$) represents EP directly to the $5\,^1P$ level. While it is possible to apply the pulsed excitation and delayed fluorescence detection technique described above to the exothermic reaction that produces the $5\,^1P$ level, the analysis of the time dependence is complicated by a long radiative decay rate of $\sim 1\ \mu$s since the fluorescence is highly trapped.

B. Thermally averaged rate coefficients

The EP rate coefficients to the $5\,^1P$ and $6\,^1S$ levels can be taken from Kelly *et al.* [6], where the $5\,^1P$ fluorescence they observed was thought to originate from the $6\,^1S$ level. The 1.1×10^{-10} cm^3 s^{-1} ($\pm 40\%$) at 700 K thermally averaged rate coefficient that they determined represents this sum, since the branching ratio from the $6\,^1S$ level to the $5\,^1P$ level is 1. Since the $5\,^3P$ atoms are initially velocity selected in the direction of the laser, xenon is added to the cell to create a thermal velocity distribution of colliding $5\,^3P$ atoms. Then, the rate coefficient measured by Kelly *et al.* can be used to find the independent rate coefficient for Eqs. (1) and (2). We measure the ratio of 461-nm fluorescence from the $5\,^1P$ level to 432-nm fluorescence from the $9\,^1P$ level excited by the probe laser to obtain the rate coefficient for each EP process. At higher xenon pressures (>2 Torr), quenching of the $9\,^1P$ level becomes significant, and these results are also used to determine a rate coefficient for the quenching of the $9\,^1P$ level by xenon. At these xenon pressures, no evidence has been found for quenching of the more tightly bound $6\,^1S$ and $5\,^1P$ levels. Previous work demonstrated that fine-structure changing collisions are negligible for the xenon pressures we utilize [18], so this experiment measures EP from collisions between a pair of $5\,^3P_1$ atoms.

Since EP to the $6\,^1S$ level is detected with a probe laser, the fraction excited to the $9\,^1P$ state by the probe laser and the detection efficiency for the measured $9\,^1P \rightarrow 4\,^1D$ fluorescence must be known to calculate the ratio of rate coefficients for EP to $5\,^1P$ and $6\,^1S$ levels. Calculations of strontium atomic transition probabilities yield 1.61×10^6 s^{-1} for the $6\,^1S \rightarrow 9\,^1P$ probe transition and a radiative branching ratio (B) of 0.426 from the $9\,^1P$ level into the measured 432-nm transition [9]. The probe beam is attenuated so that the 432-nm fluorescence from the $9\,^1P$ level is linear in probe laser intensity, and the pump rate W is calculated from $W=\sigma F$, where σ is the photoabsorption cross section calculated from the transition probability and Doppler line shapes, and F is the photon flux calculated from a laser power measurement. The detector efficiency differs by less than 10% for the photons at 432 and 461 nm.

For steady-state excitation and a pump laser broadened to a width of 100 MHz and tuned near the center of the $5\,^3P$ excitation line, the ratio of 461-nm EP fluorescence to 432-nm EP fluorescence as a function of xenon pressure is shown in Fig. 6. For low xenon pressures, the 432-nm signal increases with pressure compared to the 461-nm fluorescence, since velocity changing collisions increase the number of $5\,^3P$ atoms with above-threshold collision velocities. At xenon pressures above ~ 10 Torr, the $9\,^1P$ level is partially quenched before it radiates, and the ratio of the 432-nm $9\,^1P$ signal to the 461-nm $5\,^1P$ signal decreases. To obtain the ratio of rate coefficients, these data are fit to the following calculation.

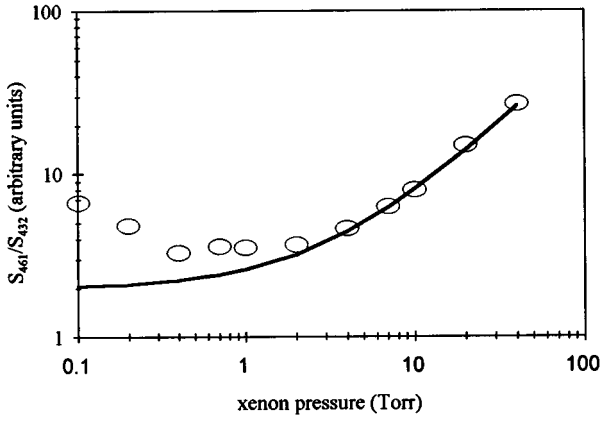

FIG. 6. The circles represent the ratio of 461-nm EP fluorescence from the $5\,^1P$ level (S_{461}) to 432-nm EP fluorescence from the $9\,^1P$ level (S_{432}) vs xenon pressure. This behavior results from quenching of the $9\,^1P$ level by collisions with xenon. The solid line is $(1+k_q n_{\text{xenon}})/\Gamma_9 1_p$, where the quenching coefficient k_q is adjusted to provide a fit to the data for pressures between 10 and 100 Torr.

For this experiment, the ratio of rate coefficients is found from the solution of three coupled rate equations that describe the evolution of the $5\,^1P$, $6\,^1S$, and $9\,^1P$ levels when the $5\,^3P$ atoms are thermalized,

$$0=\frac{d}{dt}\,n_{6\,^1s}=+\frac{1}{2}\,k_{6\,^1s}(n_{5\,^3P})^2-n_{6\,^1S}[\Gamma_{6\,^1S}+W], \quad (6a)$$

$$0=\frac{d}{dt}\,n_{5\,^1P}=+\frac{1}{2}\,k_{5\,^1P}(n_{5\,^3P})^2-n_{5\,^1P}\Gamma_{\text{eff}\,5\,^1P}, \quad (6b)$$

$$0=\frac{d}{dt}\,n_{9\,^1P}=+Wn_{6\,^1S}-n_{9\,^1P}[\Gamma_{9\,^1P}+k_q n_{\text{xenon}}+W], \quad (6c)$$

where k_q is the quenching rate coefficient of the $9\,^1P$ level by xenon, and the radiative decay rates are $\Gamma_{9\,^1P}=2.3\times10^7$ s^{-1} and $\Gamma_{6\,^1S}=1.9\times10^7$ s^{-1}. The pump rate is calculated to be $W\approx10^6$ s^{-1}, and the effective radiative rate of the highly trapped $5\,^1P$ fluorescence is calculated for a cylindrical geometry [19] to be $\Gamma_{\text{eff}\ 5\,^1P}\sim10^6$ s^{-1}. The fluorescence intensity I_j is proportional to $n_j B_j \Gamma_j$, so the ratio of rate coefficients can be written as

$$\frac{k_{6\,^1S}}{k_{5\,^1P}}=\frac{I_{9\,^1P}}{I_{5\,^1P}}\,\frac{[\Gamma_{9\,^1P}+k_q n_{\text{xenon}}+W]}{\Gamma_{9\,^1P}}\,\frac{[\Gamma_{6\,^1S}+W]}{W}\,\frac{B_{5\,^1P}}{B_{9\,^1P}}$$
$$=0.01\pm30\%, \quad (7)$$

and $k_{6\,^1S}=1.1\times10^{-12}\pm50\%$ cm^3 s^{-1}.

At large xenon pressures, when $k_q n_{\text{xenon}} \gg \Gamma_{9\,^1P}$, the rate equations yield $1/n_{9\,^1P} \propto k_q n_{\text{xenon}}$, and the inverse of the

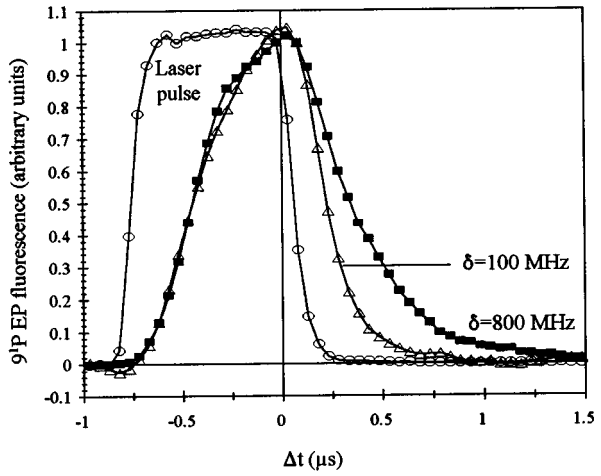

FIG. 7. 432-nm EP fluorescence from the $9\,^1P$ level vs Δt, when the $5\,^3P$ level is laser excited with a 1.0-μs pulse. The excitation pulse (circles), which is measured from scattered 689-nm light when the pump laser is tuned off resonance, ends at $\Delta t=0$. The EP fluorescence is measured for below-threshold detunings of the pump laser (triangles) and above-threshold detunings (squares). All signals have been normalized to 1 at $\Delta t=0$. At $\Delta t=1.5$ μs, the 689-nm $5\,^3P$ level fluorescence (not shown) drops less than 5% from its peak.

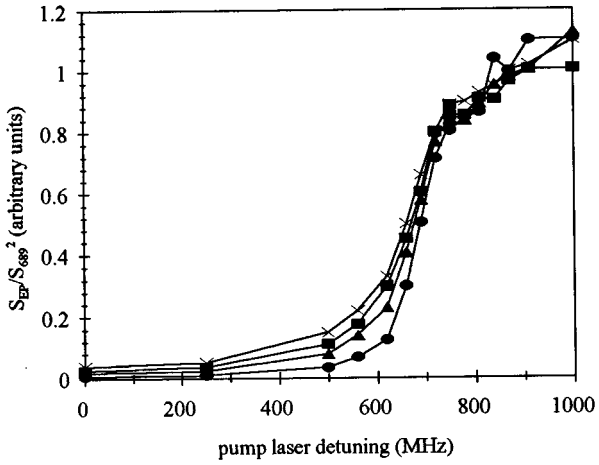

FIG. 8. The measured apparent EP rate coefficient, $k_a(\delta,t)$, vs pump laser detuning for a steady state experiment (crosses) and for $\Delta t=0.6$ μs (circles), 0.4 μs (triangles), and 0.1 μs (squares). $k_a(\delta,t)$ is obtained by dividing the 432-nm EP signal from the $9\,^1P$ level with the square of the increase during the laser pulse of the 689-nm fluorescence from the $5\,^3P$ level as described above.

432-nm $9\,^1P$ signal is linear in rare gas pressure with slope k_q. A linear fit to the ratio of fluorescence signals at xenon pressures above 1 Torr indicates a quenching rate coefficient of the $9\,^1P$ level by xenon of 5×10^{-10} cm^3 s^{-1}, which is consistent with measurements for states with similar binding energy [20].

C. Velocity dependence of EP to the $6\,^1S$ level

The velocity dependence of the EP reaction described by Eq. (1) is measured using the pulsed excitation and delayed fluorescence detection technique, where the EP signal divided by the square of the increase during the laser pulse of the $5\,^3P$ fluorescence is measured versus δ (laser detuning) and Δt (time following laser pulse). Experimental checks have been performed to remove possible systematic errors introduced by the measurement method. When two 432-nm interference filters with 10-nm bandwidths are placed on the PMT, a signal is observed only when the probe laser is tuned near the resonance of the $6\,^1S\rightarrow9\,^1P$ transition and the pump laser is tuned near the intercombination line in strontium that excites the $5\,^3P$ level. Although each 432-nm filter transmits only 3×10^{-5} of the 461-nm signal, two filters are necessary to isolate the 432-nm signal since the signal at 461 nm from the exothermic EP reaction is much stronger. Since the 461-nm fluorescence is radiatively trapped and $\tau_{9\,^1P}\ll\tau_{\mathrm{eff}\ 5\,^1P}$, the ratio of 461-nm fluorescence to 432-nm fluorescence increases with Δt.

The time-dependent 432-nm fluorescence due to EP to the $6\,^1S$ state is shown in Fig. 7 for the 689-nm pump laser tuned above ($\delta=800$ MHz) and below ($\delta=100$ MHz) the threshold detuning, and the signals are normalized to 1 at $\Delta t=0$. The rise and fall times of the laser pulse are determined primarily by an amplifier with a 0.1-μs integration time constant on the input of the transient digitizer. The EP fluorescence decays more rapidly (triangles in Fig. 7) when the pump laser is tuned below threshold, due to the narrowing of the $v_\perp$ distribution, and in either case the EP signal decays effectively to zero in $\Delta t\lesssim1.5$ μs. Total fluorescence from the $5\,^3P$ level is not shown but decays less than 10% in the 2 μs following the end of the pulse shown in Fig. 7. In most EP experiments, the EP fluorescence is proportional to the square of the fluorescence from the collision products, whereas the EP fluorescence here decays considerably more rapidly than the square of the total $5\,^3P$ fluorescence. This occurs because the $5\,^3P$ atoms spread from a small volume after they are excited by the laser pulse, and their density falls off rapidly in time. The total EP rate is roughly proportional to the integral over the probe volume of the square of the $5\,^3P$ density, so the EP fluorescence decays rapidly as a consequence of this rapidly decreasing density of $5\,^3P$ atoms within that volume. Since fluorescence from the $5\,^3P$ level is collected from the entire cell, the signal from this level is independent of spatial distribution within the cell and its time dependence is not relevant to the analysis of the EP signals in this experiment.

The laser detuning dependence to the measured EP rates is symmetric about zero detuning when measurements are made in isotopically enriched strontium, so only positive detunings are presented here. For each laser detuning, the EP signals are divided by the square of the increase during the laser pulse of the 689-nm fluorescence from the $5\,^3P$ level. As noted above, this fluorescence comes from the entire cell, but the increase during the laser pulse is proportional to the number of $5\,^3P$ atoms excited within the detection volume excited by the laser pulse. Dividing by the square of this quantity yields an apparent EP rate coefficient k_a from the EP signal. Figure 8 shows k_a versus laser detuning, for $\Delta t=0.1$ μs (squares), 0.4 μs (triangles), and 0.6 μs (circles). While data are recorded at later times as well, the expected improvement in velocity resolution is obscured by the reduc-

tion in S/N: Signals measured at $\Delta t > 1.5$ μs are $<1/100$ of their peak values (see Fig. 7). The data sets shown in Fig. 8 have been normalized to 1 at a detuning of 900 MHz so that the shape of the EP signal versus δ can be easily observed. The improvement in velocity resolution can be seen in Fig. 8 by comparing the width of the rise in EP near 700 MHz for the transient experiment to the steady-state experiment, where the velocity resolution is determined by the full thermal distribution of transverse collision energies. The steepness of the rise in k_a in the vicinity of the threshold will be used below to assess the experimentally achieved velocity resolution.

V. DISCUSSION

Physical insights into the collision process studied here can be obtained by comparing the measured cross section as a function of collision energy to simple models involving one pair of potential energy curves. Such models are relevant, despite the many molecular potential curves that branch from a pair of $5\,^3P$ excited states, because the $6\,^1S_0+5\,^1S_0$ final state connects to only two Σ molecular potential curves ($^1\Sigma_g^+$ and $^1\Sigma_u^+$), and these are expected to have similar shapes. In the analysis below, we will consider them to be the same, and label the exit-channel molecular state $^1\Sigma^+$.

The principle of microscopic reversibility can be used with the Langevin model, which is frequently used to analyze the energy dependence of collision cross sections in exothermic ion-molecule scattering [21], to describe the relationship between $\sigma(E)$ and $^1\Sigma^+(R)$. While this model is useful in treating the conditions necessary to overcome the long-range angular-momentum energy barrier, it does not explain subsequent events, such as the energy dependence of curve-hopping probabilities, which may be critical in determining whether or not a reaction occurs. The interatomic velocity v_c at the curve crossing R_c is proportional to $(E-E_c)^{1/2}$, where E_c is the energy at R_c and E is the kinetic energy of the colliding $5\,^3P$ atoms. If the crossing occurs well below E_0, as shown in the hypothetical molecular potential curves in Fig. 9, then v_c varies slowly with the excess kinetic energy $E_2=E-E_0$. This assumption is not unreasonable, since the measured sharp rise at the threshold energy indicates that $E_c<E_0$.

The Langevin model determines the energy dependence of an exothermic collision by considering the centrifugal barrier that is formed when atoms collide at impact parameter b. As two atoms approach with kinetic energy E_2 on potential $V_2(R)$, as shown in Fig. 9, radial kinetic energy of the atoms is transferred to centrifugal energy, and this creates an additional centrifugal energy barrier to the reaction. Thus, the potential energy can be represented by an effective potential $V_{\rm eff}(R,E_2)=V(R)+E_2(b/R)^2$. The location of $R_{\rm max}(E_2)$, the position where $V_{\rm eff}(R,E_2)$ has a local maximum equal to E_2, yields the largest b value $[b_{\rm max}(E_2)]$ for which the pair can reach the small-R region and induce the reaction. For $b<b_{\rm max}$, the particles ''spiral in'' to small R, and the reaction occurs. Thus, $\sigma(E)=\pi[b_{\rm max}(E_2)]^2$. For an exothermic reaction with an attractive initial state $V(R)=-C_s/R^s$, where $s>2$, an analytic solution for $b_{\rm max}(E_2)$ is found that leads to $\sigma(E_2)\propto E_2^{-2/s}$. This result gives the familiar $E^{-1/2}$ dependence to the cross section for exothermic ion-molecule reactions, where the long-range interatomic potential has a $V(R)\propto -1/R^4$ dependence.

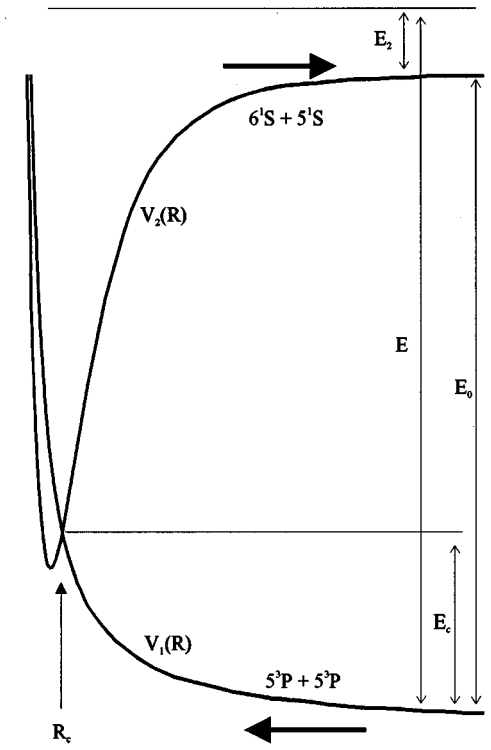

FIG. 9. Hypothetical potential energy curves plotted vs internuclear distance R for an EP reaction between two $5\,^3P$ atoms with kinetic energy E that produce a $6\,^1S$ and $5\,^1S$ atom. The collisionally produced state exits with energy $E_2=E-E_0$, where E_0 is the separated atom limit of the electronic energy difference between the collision pairs and the collisionally produced levels. E_c is the energy at the curve crossing.

The energy dependence to the cross section for an endothermic reaction can be found using the above result and the principle of detailed balance [22], which states $E_1\sigma_{1-2}g_1=E_2\sigma_{2-1}g_2$, where the g_i are the statistical weights of the molecular states and E_1 is the kinetic energy E of the collision partners. If E_2 does not exceed the angular-momentum barrier, the atoms cannot separate to the upper state, so the same $b_{\rm max}(E_2)$ applies to both endothermic and exothermic reactions. For atoms that approach in state 1 with initial kinetic energy E, as shown in Fig. 9, the cross section for an endothermic reaction is $\sigma_{1-2}=\sigma_{2-1}(E_2/E)(g_2/g_1)$. In this experiment, the $6\,^1S_0+5\,^1S_0$ upper state has a statistical weight of 2, and the $5\,^3P_1+5\,^3P_1$ lower state has a statistical weight of 9. If we assume the upper-state interatomic potential has the form $V(R)\propto -R^{-s}$, then the above exothermic σ_{2-1} in the detailed balance relation yields the endothermic cross section $\sigma_{1-2}\propto(E-E_0)^{1-2/s}/E$. This yields a hard-sphere result when $s=\infty$, $\sigma\propto(E-E_0)/E$, which is equivalent to the line-of-centers model [21,22]. Figure 10 shows cross sections for an endothermic reaction with a threshold at E_0 and an upper state potential curve of the form $V_2(R)\propto -1/R^s$ with $s=4$, 6, and ∞.

The experimentally determined energy dependence of the collision cross section can be compared to the theory illus-

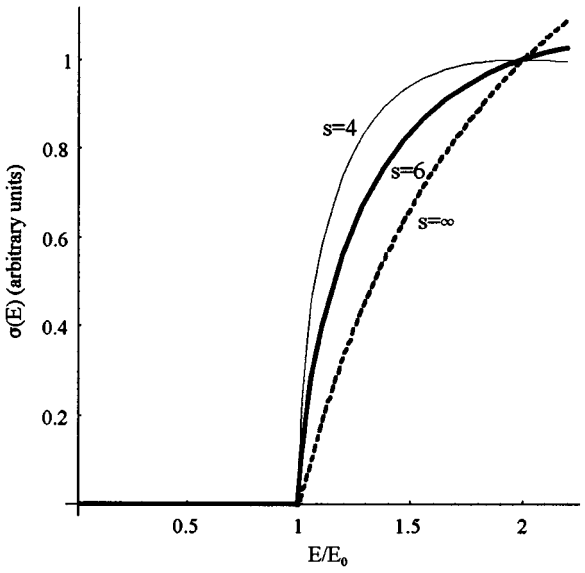

FIG. 10. The energy dependence of several model cross sections using the Langevin model and microscopic reversibility, assuming interatomic potentials of the form $V(R) \propto -1/R^s$.

trated in Fig. 10. Since the collision velocity is almost entirely determined by the collision velocity in the laser direction for above-threshold collisions, the energy dependence of the apparent collision cross section σ_a can be written as $\sigma_a(E) \propto k_a(E)/\sqrt{E}$, where $E \approx E_z$. Figure 11 shows that the apparent cross section rises steeply at threshold and is nearly energy independent for collision energies from $\sim E/E_0 = 1.1$ up to twice the threshold energy. Using the 1.1×10^{-12} cm^3 s^{-1} thermal rate coefficient for EP from a pair of $5\,^3P$ atoms to the $6\,^1S$ level and the energy dependence to the cross section, the EP cross section above threshold is determined. For a collision cross section (σ_0) that is zero

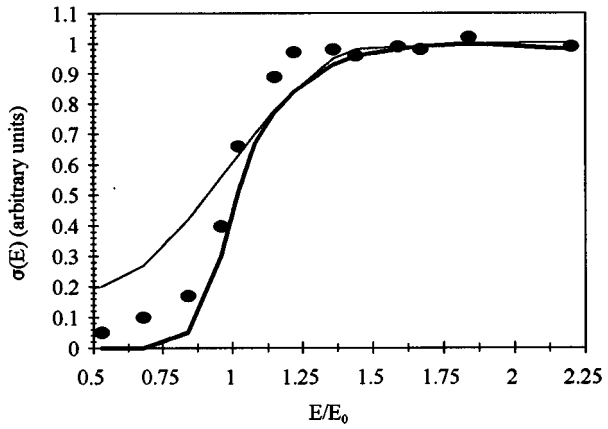

FIG. 11. The experimentally measured energy-dependent cross section for a steady-state experiment (thin line) and for an experiment where $v_\perp$ is narrowed by pulsed excitation followed by delayed fluorescence detection (points). The thick line is the model with $V(R) \propto -1/R^4$ convoluted with the theoretically determined velocity resolution. The energy threshold for this reaction is $E_0 = 1583$ cm^{-1}.

below a threshold energy E_0 and constant above this threshold, integration of the product of the cross section and the collision velocity over the thermal velocity distribution yields the thermal rate coefficient,

$$k_{\text{thermal}} = \sigma_0 \left(\frac{8kT}{\pi\mu} \right)^{1/2} \left(1 + \frac{E_0}{kT} \right) e^{-E_0/kT}, \tag{8}$$

where the expression $(8kT/\pi\mu)^{1/2}$ is the mean thermal velocity. For this reaction, the cross section is calculated with Eq. (8) to be $\sigma_0 \approx 6 \times 10^{-17}$ cm^2.

The close fit between the experimental results and the calculated apparent cross section convoluted with the theoretically determined energy resolution for $V_2(R) \propto -1/R^4$ (Fig. 11) suggests that the energy dependence to this collision can be roughly described by a $-1/R^4$ molecular potential for the upper $^1\Sigma$ state in the region of the centrifugal barrier. Using microscopic reversibility and the Langevin model, a potential of the form $V_2(R) \propto -1/R^s$ has a binding at $R_{\max}$ of $V_2(\infty) - V_2(R_{\max}) = 2E_2/(s-2)$, or a binding of E_2 for $s=4$. Thus, the data essentially test the shape of $V_2(R)$, where it is bound by E_2. In the present experiment, where the energy resolution is ~ 100 cm^{-1} (discussed below) and the range of collisional kinetic energies is 3200 cm^{-1}, this is $V_2(\infty) - V_2(R_{\max}) = 100 - 3000$ cm^{-1}. In Fig. 11, the difference between the theoretical model and the data is not surprising, as the molecular potential curve of the exit channel is not likely to be described exactly by a simple power law.

The experimentally determined apparent cross section has a large below-threshold tail, which is not explained by the theoretical model, regardless of the velocity dependence of the cross section above threshold. The below-threshold cross section at $\sim 0.7E_0$ in Fig. 11 is about 10% of the above-threshold value, whereas the theory predicts that it should be less than 1%. This is evidence that the measured velocity resolution is degraded in a way that has not been included in the theory, which considers the velocity resolution to be solely determined by the transverse velocity distribution. Velocity-changing collisions of $5\,^3P$ atoms are a possible explanation for the observed low-velocity tail in Fig. 11. Resonance broadening is the dominant velocity-changing mechanism. From the 4×10^{-9} cm^3 s^{-1} self-broadening rate coefficient [23], these excitation exchange collisions that redistribute velocity are calculated to contribute about 1% of the EP signal, whereas 10% below-threshold tails are observed. Gibble and Gallagher [24] studied velocity changing collisions between rare-gas atoms and ground-state rubidium atoms, and the rate coefficients they measured for the large velocity changes that would explain the below-threshold tail in these data are smaller than the above self-broadening rate coefficient. Radiative redistribution could also be discussed as a possible mechanism for destroying velocity selection. When a $5\,^3P$ atom emits a photon, there is a chance that a ground-state strontium atom, with a thermal velocity that is not controlled by the laser, is excited by the emitted photon. Using Beer's law and typical strontium densities, it is calculated that fewer than 0.8% of the emitted photons are absorbed over a 100-μm radius detection volume.

The width of the step in the cross section near threshold in Fig. 11 is used to assess the energy resolution. Energy reso-

lution is defined here to be the FWHM of the change in the EP cross section from $E/E_0=0$ to $E/E_0=1$. The above theory, which includes the effects of the transverse velocity distribution upon the collision rate, predicts an energy resolution of $\sim 50\ \mathrm{cm}^{-1}$, whereas the experimentally measured energy resolution is $\sim 100\ \mathrm{cm}^{-1}$. At the cell, the laser beams are measured to be 150 μm$\times$300 μm FWHM, with roughly Gaussian spatial distributions in each dimension, whereas the theory assumed (for ease of calculation) a laser beam with a 100-μm radius step-function profile. Hence, the difference between theory and experiment in the laser beam spatial distribution might explain the discrepancy in the energy resolution. This discrepancy, which is reduced when a larger laser beam radius is used in the theory, is consistent with the atoms staying in the beam longer than the model assumes. Pulsed excitation with delayed fluorescence detection is shown in Fig. 11 to improve the energy resolution by a factor of four from the $\sim$400-cm^{-1} energy width measured in the steady-state experiment.

Further insight into the collision is revealed by the measured cross section for reaction (1) of 0.6 $\mathrm{Å}^2$, which is $\sim \pi R_c^2/50$ for the expected $R_c \sim 3$ Å. If a pair of colliding $^3P_1$ atoms couples to all the molecular curves from the ^3P multiplet, then the cross section for reaction (1) is weighted by the 2/81 statistical branching of a pair of ^3P atoms to the $^1\Sigma^+$ potentials. Thus, if nothing extraordinary occurs in the fine-structure recoupling region, the hopping probability at an avoided $^1\Sigma^+$ crossing is near maximum. As a result, the hopping probability at R_c is expected to be nearly independent of v_c or E.

VI. CONCLUSIONS

This study of the velocity dependence of EP in strontium has produced several interesting results. The collisional production of the $5\,^1P$ level from a pair of $5\,^3P$ atoms, which was previously thought not to occur due to the large energy defect ($\sim$1 eV), has a large thermally averaged rate coefficient ($1.1\times10^{-10}\ \mathrm{cm}^3\,\mathrm{s}^{-1}$). The rate coefficient for EP from a pair of $5\,^3P$ atoms to the $6\,^1S$ state is small ($1.1\times10^{-12}\ \mathrm{cm}^3\,\mathrm{s}^{-1}$), and the above-threshold cross section for this process is approximately $6\times10^{-17}\ \mathrm{cm}^2$. The velocity dependence to the cross section of this EP reaction rises steeply at threshold and is nearly flat for collision energies slightly above threshold to twice the threshold energy. This result is shown to be consistent with an avoided crossing well below threshold and an upper $6\,^1S+5\,^1S$ molecular state potential that varies approximately as $V(R)\propto -1/R^4$ in the region where $V(R)$ is bound by the excess collisional kinetic energy.

We have devised and demonstrated a pulsed excitation and delayed fluorescence detection technique that achieves a major improvement in collisional energy resolution in a cell, which is normally limited to kT in velocity-selective collision experiments. This technique is applicable to studies of the velocity dependence of collisions in vapor cells. We have calculated the time-dependent transverse velocity distribution, and this is used with a collision model to explain the data. In a vapor cell with high densities of strontium ($\sim 3\times10^{13}\ \mathrm{cm}^{-3}$), we measure the velocity dependence of an EP reaction with a 0.6-$\mathrm{Å}^2$ cross section, with a velocity resolution four times better than what would be measured if the transverse velocity were not controlled.

ACKNOWLEDGMENT

This work was supported by National Science Foundation Grant No. PHY90-12244 to the University of Colorado.

[1] Z. L. Jabbour, R. K. Namiotka, J. Huennekens, M. Allegrini, S. Milosevic, and F. de Tomasi, Phys. Rev. A **54**, 1372 (1996).
[2] T. Walker and P. Feng, in *Advances in Atomic, Molecular, and Optical Physics*, edited by B. Bederson and H. Walther (Academic, San Diego, 1994), Vol. 24, p. 125.
[3] J. A. Neuman, A. Gallagher, and J. Cooper, Phys. Rev. A **50**, 1292 (1994).
[4] H. G. C. Werij, M. Harris, J. Cooper, and A. Gallagher, Phys. Rev. A **43**, 2237 (1991).
[5] J. H. Nijland, J. A. deGouw, H. A. Dijkerman, and H. G. M. Heideman, J. Phys. B **25**, 2841 (1992); H. R. Thorsheim, Y. Wang, and J. Weiner, Phys. Rev. A **41**, 2873 (1990).
[6] J. F. Kelly, M. Harris, and A. Gallagher, Phys. Rev. A **28**, 1225 (1988).
[7] N. Boutassetta, A. R. Allouche, and M. Aubert-Frecon, Phys. Rev. A **53**, 3845 (1996).
[8] J. Apt and D. E. Pritchard, Phys. Rev. Lett. **37**, 91 (1976).
[9] H. G. C. Werij, C. H. Greene, C. E. Theodosiou, and A. Gallagher, Phys. Rev. A **46**, 1248 (1992).
[10] P. Meystre and M. Sargent III, *Elements of Quantum Optics* (Springer-Verlag, Berlin, 1991).
[11] C. E. Wieman and L. Hollberg, Rev. Sci. Instrum. **62**, 1 (1991).
[12] A special thanks to N. Mackie, from L. Hollberg's NIST research group, who coated the diodes.
[13] G. H. Newsom, S. O'Connor, and R. C. M. Learner, J. Phys. B **6**, 2162 (1973).
[14] C. E. Moore, in *Atomic Energy Levels*, NBS Circular No. 467 (U.S. G.P.O., Washington, D.C., 1949).
[15] A. N. Nesmayanov, *Vapor Pressure of the Elements* (Academic, New York, 1963).
[16] J. A. Neuman, P. Wang, and A. Gallagher, Rev. Sci. Instrum. **66**, 3021 (1995).
[17] P. S. Danner, J. Am. Chem. Soc. **46**, 2382 (1924); J. Langlais and R. Harris, Can. Metallurgical Quarterly **31**, 127 (1992).
[18] J. F. Kelly, M. Harris, and A. Gallagher, Phys. Rev. A **37**, 2354 (1988).
[19] T. Holstein, Phys. Rev. **83**, 1159 (1951).
[20] R. W. Schwenz and S. R. Leone, Chem. Phys. Lett. **133**, 433 (1987).

[21] J. I. Steinfeld, J. S. Francisco, and W. L. Hase, *Chemical Kinetics and Dynamics* (Prentice-Hall, Englewood Cliffs, NJ, 1989).

[22] R. D. Levine and R. B. Bernstein, *Molecular Reaction Dynamics and Chemical Reactivity* (Oxford University Press, New York, 1987).

[23] J. K. Crane, M. J. Shaw, and R. W. Presta, Phys. Rev. A **49**, 1666 (1994).

[24] K. E. Gibble and A. Gallagher, Phys. Rev. A **43**, 1266 (1991).